Journal of Orthopaedic Translation 50 (2025) 223–234

Contents lists available at ScienceDirect

Journal of Orthopaedic Translation

journal homepage: www.journals.elsevier.com/journal-of-orthopaedic-translation

Original Article

Moldable self-setting and bioactive bone wax for bone hemostasis and defect repair

Ziyang Liu [a,1], Chuang Liu [b,1], Huan Zhou [b,*,1], Chunyong Liang [b], Wei Chen [c,d,e], Yanjie Bai [f], Xinlong Ma [a,**], Yingze Zhang [c,d,e,***], Lei Yang [b,****]

[a] Department of Orthopedics, Tianjin Hospital, Tianjin, China
[b] Center for Health Sciences and Engineering, Hebei Key Laboratory of Biomaterials and Smart Theranostics, School of Health Sciences and Biomedical Engineering, Hebei University of Technology, Tianjin, China
[c] Department of Orthopaedic Surgery, The Third Hospital of Hebei Medical University, No.139 Ziqiang Road, Shijiazhuang, China
[d] Key Laboratory of Biomechanics of Hebei Province, Orthopaedic Research Institution of Hebei Province, No.139 Ziqiang Road, Shijiazhuang, China
[e] NHC Key Laboratory of Intelligent Orthopaedic Equipment, The Third Hospital of Hebei Medical University, No.139 Ziqiang Road, Shijiazhuang, China
[f] Department of Chemical Engineering, Hebei University of Technology, Tianjin, China

ARTICLE INFO

Keywords:
Bone bleeding
Bone wax
Hemostasis
Osteogenesis

ABSTRACT

Objective: Bone injury complicated with bleeding and irregular shaped defect are challenging in orthopedic surgery and practices due to the lack of reliable hemostasis and simultaneous defect repair strategy. Bone wax is a century-old biomaterial for bleeding management in orthopedic surgery, characterized with ready-to-use advantage but the risk of failed bone reunion due to the biological inertness and non-degradability. In current work, integration of bioceramic cement and premixed concept was motivated to prepare a in situ self-setting bioactive calcium phosphate based bone wax (CaPBW) for bone hemostasis and defect repair.

Methods: A moldable, in situ self-setting bioactive CaPBW with a novel formulation of calcium phosphate cement (CPC), monetite (DPCA) granules, modified starch and polyethylene glycol (PEG) was developed for bone hemostasis and defect repair. The CaPBW material was evaluated by characterization, physical and chemical properties, biocompatibility, osteogenic ability and hemostatic ability.

Results: CaPBW adopted the ready-to-use feature of traditional bone wax, showing feasibility in shape molding and defect sealing. When interacted with physiological fluid like blood, CaPBW could transformed from putty to solid state within tens of minutes due to the gradual PEG-water exchange and CPC hydration, providing mechanical stability for bleeding clotting and bone defect filling. *In vitro* studies revealed the superiority of CaPBW over bone wax in blood coagulation and osteoblast differentiation, along with hemocompatibility and osteogenesis confirmation. *In vivo* studies demonstrated the reliability of CaPBW in hemostasis and bone regeneration compared to traditional bone wax, promoting the efficacy of bone bleeding and new bone formation.

Conclusion: As compared to traditional bone hemostatic agent bone wax, CaPBW not only preserved its advantages in handling and defect sealing, but also provided platform for temporary physical support and bone regeneration acceleration.

The translational potential of this article: The integrated design of osteogenesis and hemostasis makes CaPBW have the dual functions as bone hemostasis material and artificial bone substitute. CaPBW therefore demonstrates a strategy of next-generation bone wax with high translational potential for orthopedic surgery.

* Corresponding authors. Center for Health Sciences and Engineering, Hebei Key Laboratory of Biomaterials and Smart Theranostics, School of Health Sciences and Biomedical Engineering, Hebei University of Technology, Tianjin, 300131, China.

** Corresponding author. Department of Orthopaedic Surgery, The Third Hospital of Hebei Medical University, No.139 Ziqiang Road, Shijiazhuang, 050051, China.

*** Corresponding authors. Department of Orthopedics, Tianjin Hospital, Tianjin, 300211, China.

**** Corresponding author. Center for Health Sciences and Engineering, Hebei Key Laboratory of Biomaterials and Smart Theranostics, School of Health Sciences and Biomedical Engineering, Hebei University of Technology, Tianjin, 300131, China.

E-mail addresses: zhouhuan@hebut.edu.cn (H. Zhou), maxinlong8686@sina.com (X. Ma), yzling_liu@163.com (Y. Zhang), ylei@hebut.edu.cn (L. Yang).

[1] Ziyang Liu, Chuang Liu, and Huan Zhou made equal contribution to this work and should be considered co-first authors.

https://doi.org/10.1016/j.jot.2024.11.009
Received 4 March 2024; Received in revised form 4 November 2024; Accepted 28 November 2024

1. Introduction

Natural bone is a mineralized and vascularized connective tissue in body, characterized with functions in structural support, organ protection, and mineral reservoir. When faced with severe trauma and critical surgical scenarios, impaired or incised bone usually encounters with mechanical stability loss, irregular defect shape, bone regeneration failure and bleeding [1–3]. For example, in open-wedge high tibial osteotomy (HTO) for unicompartmental knee osteoarthritis treatment, a wedge osteotomy gap was created to provide symptomatic relief and postpone joint replacement need [4,5]. Nevertheless, this surgery can cause extensive intraoperative and postoperative bleeding due to medullary cavity exposure in osteotomy gap, in which total hemoglobin loss is estimated to be approximately 1.7–4.1 g/dL, with a 1.5 %–6 % incidence of unintended postoperative hematoma and a 5 %–7 % incidence of wound complications [6–8]. Moreover, 20 %–30 % hinge fracture and up to 4.6 % nonunion rate were reported due to the removal of large sized bone tissue [9–12].

In such cases, external intervention must be urgently applied for bleeding bone defect management. Surgeons have sealed the bone gap using autogenous bone or artificial bone material, purposed to shorten the time for bony union [13,14]. However, known agents in form of granules, spacers, chips, paste, or putty fail to simultaneously adapt to the needs of structure integrity and stability restoration in time [15,16]. In spite of that, it is also important to stop bleeding in the bone defect for clinical outcome improvement. In clinical practice, the mostly acknowledged bone hemostatic agent is bone wax, highlighted with its excellent hemostatic capacity, ease of use, and low cost. However, this century-old agent is often criticized for its risks of allergic reactions, foreign body rejection, infection and bone regeneration failure at the surgical site [17]. Meanwhile, strategies based on external pressure and absorption is accompanied with excessive plasma absorption and low success rate of hemostasis, along with limited adaption to the irregular sized rigid bone defect. Some emerging absorbable bone wax alternatives launched in recent years are still far away from worldwide clinical recognition due to limited osteogenic capacity, poor mechanical performance, or entirely different operation procedure to bone wax [17].

With progressed understanding the mechanism of bone hemostasis and repair as well as the medical needs, it is desperately essential to develop a more reliable material for bone hemostasis and defect repair, with the preservation of the attractive characteristics of traditional bone wax. Bioceramic based cement allows for shape adaptation during injection and strength support after self-curing. However, this kind of materials need to be manually prepared on site and immediately implanted during its working time, resulting in extra workload for surgeons and limited adaption to unpredictable bleeding during surgery. Meanwhile, in a recent work by our group, a ready-to-use bone wax like putty based on monetite (DCPA, $CaHPO_4$) granules, modified waxy starch and water was proposed, revealing impressive cohesive, malleable, tissue adhesive and liquid sealing abilities [18]. However, long-term fully exposure of starch and DCPA to water may result in gradual hydrolysis of these materials, causing product quality control concern during storage.

On the basis of these efforts, integration of bioceramic cement and premixed concept was motivated to prepare a in situ self-setting bioactive calcium phosphate based bone wax (CaPBW) for bone hemostasis and defect repair in current work. On one hand, with the incorporation of plastic polyethylene glycol (PEG) the as-prepared CaPBW could be malleable and smeared into irregular sized bone defect like bone wax in the absence of water, along with the self-curing behavior stimulated when in contact with body fluid. On the other hand, this as-prepared CaPBW revealed capabilities of hemostasis and bone regeneration in both *in vitro* and *in vivo* testing, paving the possibility of high-quality bleeding bone management in situ.

2. Materials and methods

2.1. Preparation of bone putty

In this study, the formulation of calcium phosphate cement (CPC) powder was a mixture of alpha-tricalcium phosphate (α-TCP) and dicalcium phosphate dihydrate ($CaHPO_4{\cdot}2H_2O$, DCPD) at a mass ratio of 9:1 [19].

For preparing DCPA granules, a setting solution of 6 g $NaHCO_3$, 2.05 mL of DI water, and 12.95 mL of H_3PO_4 (85 wt%) were firstly prepared. Then 15 mL of the as prepared setting solution were manually mixed with 15.58 g of $Ca(OH)_2$ and 5 mL of DI water using an agate pestle for 10 min to form cement pastes. Sieving was performed subsequently using 60 and 80 mesh sieves to generate 200–300 μm sized DCPA granules. After settled in air for 1 h, these granules were moved to a 37 °C oven for 24 h of curing. Finally, the solidified granules were rescreened via sieving for confirming the uniformity of size distribution.

In the process of starch modification, water, waxy starch with amylopectin >90 % (Lihua starch, China), and cross-linking agent calcium nitrate (Yuanyang Bio-tech, China) were mixed in a mass ratio of 240:48:1. After 1 h of stirring at 90 °C, a cross-linked viscous gel was obtained, followed by baking in an oven at 120 °C for 12 h to remove moisture. The dried sample was milled to obtain waxy starch gel powder.

Finally, 0.4 g of CPC powders, 0.4 g of DCPA granules, 0.145 g of waxy starch gel power, and 0.05 g of sodium dihydrogen phosphate (NaH_2PO_4) were uniformly mixed using an oscillator. PEG precursor solution was prepared by mixing molten PEG 1500 and PEG 500 at 70 °C in a 4:1 mass ratio. 0.6 g of PEG precursor solution was then poured into the as-mixed powder followed by stirring to form a viscous paste. After cooling to room temperature, the mixture was solidified and a transition from paste to malleable putty was witnessed. The prepared DCPA particles and the resulting CaPBW were characterized using X-ray Photoelectron Spectroscopy (XPS, K-Alpha, Thermo Fisher Scientific, USA) and Fourier Transform Infrared Spectroscopy (FTIR, TENSOR 27, Bruker, Germany).

2.2. Material characterizations

2.2.1. Anti-collapsibility

CaPBW with initial mass recorded as M_0 was kneaded into cylinder and placed in a Petri dish (60 mm diameter) with phosphate buffered saline (PBS). The dish was moved to a shaker for shaking test to determine the anti-collapsibility of CaPBW during the exchange of PEG and water. After 10 min, the structure integrity of the CaPBW specimen was determined visually. Later, the cylinder specimen was lyophilized to a constant weight, and the mass was recorded as M_1. The mass loss caused by specimen collapse in aqueous environment was then expressed as the mass loss ate according to $(M_0 - M_1)/M_0 \times 100$ %.

2.2.2. Compressive strength

CaPBW was filled into a cylindrical mold (6 mm in diameter and 12 mm in height) for shaping. Subsequently, the samples were placed in PBS with the mold at 37 °C to process the hardening of CaPBW via the exchange between PEG and water. At different time intervals, solidified specimen was pushed out of the mold and its upper and lower surfaces were polished with 2000 grit sandpaper to make it smooth and parallel. Subsequently, compressive strength of as-prepared cylindrical specimen was tested using a universal material testing machine (HY-1080, HengYi Precision Instrument, China) with a 5 kN load cell at a cross-head speed of 1 mm/min.

2.2.3. Degradation behavior in vitro

The initial mass of CaPBW was weighed and recorded as M_0. The specimen was loaded into a test tube and the total mass was recorded as M_1. The corresponding amount of PBS (pH = 7.2–7.4) was added to the

test tube at a 1/20 g/mL ratio. The tube was then incubated at an ambient temperature of 37 °C and residual specimen at different time point was collected and lyophilized to a constant weight recorded as M_2. The mass loss rate was calculated according to $(M_1 - M_2)/M_0 \times 100$ %. In addition, the phase and morphology changes of CaPBW with time were studied using X-ray diffraction (XRD, D8 Discover, Germany) and scanning electron microscope (SEM, HITACHI S-4800, Japan).

2.3. Hemostasis ability evaluation

2.3.1. Liquid sealing capability

Acrylic tube model: In this experiment, an acrylic tube with an inner diameter of 3 mm was placed vertically and filled with water to form a 1.9 m high water column to simulate a vascular systolic pressure of 140 mmHg (18.68 kPa). One end of the acrylic tube was sealed with bone wax (W810, ETHICON™, Johnson & Johnson, USA) and CaPBW respectively, and the water leakage and fluid sealing time were recorded to determine the capability of CaPBW forming physical barrier to stop blood flow.

Long bone model: Fresh hollow pig long bones were moistened by soaking in saline solution, and the sample was applied to seal one end of the bone defect. The other end was connected to a water column at a height of 18 cm (simulating central venous pressure). The experiment was conducted to observe whether the material could adhere to the wet bone defect and maintain its integrity under water pressure.

2.3.2. Wettability

The water contact angle of bone wax and CaPBW were evaluated using a contact angle goniometer (JC2000DM, Shanghai Zhongchen, China) to compare their surface affinity to blood.

2.3.3. Platelet affinity

Pre-warmed tablets (0.2 g, 10 mm diameter) of bone wax and CaPBW were exposed to 0.5 mL of whole blood at 37 °C for platelet affinity evaluation. After 30 min of contact, free platelets on the specimen surface were washed off with PBS. The residual platelets were fixed with 2.5 % glutaraldehyde and gradually dehydrated using alcohol with concentration order increased from 40 %, 60 %, 80 %, 90 %, to 100 %. After air-drying at room temperature for 24h, specimen surface was characterized using SEM.

2.3.4. Clotting time

After immobilizing, anesthetizing, and disinfecting New Zealand rabbits, blood was collected from the carotid artery using 3.2 % sodium citrate as an anticoagulant. The anticoagulated whole blood was centrifuged at 1200G for 10 min to obtain platelet-poor plasma (PPP) from the upper layer. Both bone wax and CaPBW samples (50 mg each) were placed into 1.5 mL centrifuge tubes, washed once with physiological saline, and then 1 mL of PPP was added. PPP without any sample was used as the blank control. Three parallel samples were set for each group, and they were incubated statically at 37 °C for 60 min. After incubation, the samples were centrifuged at 3000 rpm for 10 min, and the supernatant PPP was collected. The APTT and PT values of the incubated PPP were measured using an automated coagulation analyzer (CS-5100, SYSMEX, Germany).

Activated partial thromboplastin time (APTT): The instrument automatically pipetted 0.1 mL of plasma and 0.1 mL of Actin reagent, thoroughly mixed the solution, and incubated it at 37 °C for 3 min. Then, 0.1 mL of 25 mM $CaCl_2$ solution was added, mixed, and the timing began. The instrument detected clot formation and automatically calculated the APTT.

Prothrombin time (PT): The instrument automatically pipetted 0.1 mL of plasma into the test cup and incubated it at 37 °C for 1 min. Then, 0.2 mL of Thromborel S reagent was added, thoroughly mixed, and the timing began. The instrument detected the coagulation time and calculated the PT.

2.3.5. Thromboelastography (TEG)

Following the previously described method, blood was collected from New Zealand rabbits and anticoagulated. Bone wax and CaPBW samples (50 mg each) were placed into 1.5 mL centrifuge tubes, and 1 mL of anticoagulated blood was added. The mixture was stirred using a pipette tip for thorough mixing. A blank centrifuge tube with 1 mL of anticoagulated blood was used as the control. For testing, 20 μL of 0.2 mol/L calcium chloride solution and 340 μL of the sample-treated anticoagulated blood were sequentially added to the test cup. The analysis was performed using the thrombelastograsph cogulation analyzer (TEG-5000, Haemonetics, USA) under default settings.

2.3.6. Hematolysis rate

Saline was used to prepare the extract of CaPBW or bone wax (0.1 g/mL, 37 °C, 24h). Diluted blood was prepared by mixing 8 mL of blood with 10 mL of physiological saline. 10 mL of the extract was pre-warmed at 37 °C for 30 min in a test tube, followed by mixing with 0.2 mL of diluted blood. After another 1 h incubation at 37 °C, supernatant of the mixture was harvested via by centrifugation (4000 rpm, 15min) and its absorbance at 545 nm was measured afterwards. These procedures were repeated with deionized water as the positive control group (hemolysis rate of 100 %) and pure saline as the negative control group (hemolysis rate of 0 %). The hemolysis rate could be calculated as follows: hemolysis rate % = (OD of experimental group - OD of negative group)/(OD of positive group - OD of negative group) × 100 %.

2.4. In vitro cellular tests

2.4.1. Cytocompatibility

The extract medium was obtained by immersing the test material in 37 °C Dulbecco's Modified Eagle Medium (DMEM) high glucose without added serum at 0.1 g/mL for 24 h. After centrifugation (4000 rpm, 20min), supernatant was sterilized using 0.22 μm. Complete medium was prepared by adding 10 % fetal bovine serum (FBS) (Gibco, USA) for cell culture. Standard DMEM complete medium containing 10 % FBS was used as control group for cell culture.

MC3T3-E1 cells were inoculated in 96-well plate at a density of 5000 cells per well. As-prepared medium was used for cell culture with test medium. After 1 and 3 days of cell culture, proliferation of MC3T3-E1 cells was detected using CCK-8 Cell Proliferation and Cytotoxicity Assay Kit (Solarbio, China). The absorbance at 450 nm was measured using SpectraMax M4 microplate reader (Molecular Devices, USA). The relative growth rate (RGR) of cells was calculated as follows: $RGR = (OD_{test} - OD_{blank})/(OD_{control} - OD_{blank}) \times 100$ %.

The viability of MC3T3-E1 cells exposed to material extract was also detected using Calcein/PI Cell Viability/Cytotoxicity Assay Kit (Beyotime, China). Cells were inoculated in 24-well plate at a density of 10,000 cells per well. After 3 days of cell culture, 250 μL Calcein AM/PI solution was added to each well and incubated the plate for 30 min. The live/dead staining was observed under a fluorescence microscope (DMI4000B, Leica, Germany).

2.4.2. Alkaline phosphatase (ALP) activity

The preparation method of material extract medium for testing is similar to that described in section 2.4.1 On this basis, the bone wax and CaPBW extract medium and the standard medium were supplemented with 0.01 mol/L β-glycerophosphate, 10^{-8} mol/L dexamethasone, and 50 μg/mL ascorbic acid (Solarbio, China) to formulate them into three osteoblast induction medium.

The ability of CaPBW to induce cell differentiation and ALP activity was detected using ALP staining. BCIP/NBT Alkaline Phosphatase Color Development Kit (Beyotime, China) was used for MC3T3-E1 cells with osteoblastic induction. In brief, cells were inoculated in 6-well plate at a density of 100,000 cells per well with cell culture medium replenished every 3 days. After 7 days, cells were fixed with 4 % paraformaldehyde (Solarbio, China) for 30 min and then washed with PBS. Staining

solution of 1 mL was added to each well, and ALP density was observed using a microscope (IX73, Olympus, Japan) after incubation at darkness.

2.4.3. Cell mineralization and semiquantification

The ability of the material extract to induce cell mineralization was detected using Alizarin Red S (ARS) staining. ARS Staining Kit for Osteogenesis (Beyotime, China) was used for MC3T3-E1 cells with osteoblastic induction. Cells were inoculated in 6-well plate at a density of 100,000 cells per well. Cell culture medium was changed every 3 days. After 14 days, cells were fixed with 4 % paraformaldehyde for 30 min and then washed with PBS. Staining solution of 1 mL was added to each well. After 30 min of staining, the deposited calcium was observed using a microscope (IX73, Olympus, Japan). In addition, 10 % Cetylpyridinium Chloride was added and the absorbance of the solution was measured using a microplate reader (OD at 590 nm).

2.4.4. Osteogenic mRNA expression

Cell differentiation and expression of osteogenic genes were detected by reverse transcription quantitative real-time PCR (RT-qPCR). MC3T3-E1 cells were inoculated in 6-well plate at a density of 200,000 cells per well. Cells were cultured with the extract containing osteogenic inducing components, and medium was changed every 3 days. After 7 days, Cell Total RNA Isolation Kit (Foregene, China) was used to remove DNA and extract RNA from cells. The concentration of extracted RNA was detected using Biomate 3S Spectrophotometer (Thermo Scientific, USA) with the OD_{260}/OD_{280} ratio in the range of 1.9–2.1. Subsequently, 2 μg of RNA was diluted and reverse transcribed. The cDNA synthesis reaction was performed using HiFiScript cDNA Synthesis Kit (Cwbio, China) and S1000 Thermal Cycler (Bio-Rad, USA), with reaction conditions set at 42 °C for 15 min and 85 °C for 5 min. The products were diluted, followed by primers (Sangon Biotech, China) and TB Green Premix Ex Taq (Takara, Japan) addition. Quantitative real-time PCR was performed using LightCycler 480 II (Roche, USA). Osteogenesis related genes tested in current work were osteocalcin (OCN) and osteopontin (OPN), and glyceraldehyde 3-phosphate dehydrogenase (GAPDH) was used as the reference gene to normalize their expression. Primer sequences used in PCR are shown in Table 1.

2.5. In vivo evaluations of hemostasis and osteogenesis

All protocols were performed under the guideline of the Association for Assessment and Accreditation of Laboratory Animal Care and approved by the Ethics Committee of the Orthopedic Research Institute, Tianjin Hospital (2022 Medical Ethical Review 193). The experimental animals were male SD rats weighing 200 g–230 g. According to different filling materials, rats were randomly divided into three groups: the control group, the bone wax group, and the CaPBW group. We used 2 mm diameter femoral defect model and 5 mm diameter calvarial defect model for *in vivo* hemostasis and osteogenesis experiments, respectively. Because the femoral defect can better simulate the long bone hemorrhage with opened marrow cavity, while the larger critical size defect of 5 mm in calvarium can provide better bone regeneration information [20,21].

Table 1
Primer sequences in PCR analysis.

Gene	Primer	Sequence
GAPDH	Forward	GGTGAAGGTCGGTGTGAACG
	Reverse	CTCGCTCCTGGAAGATGGTG
OCN	Forward	AGACTCCGGCGCTACCTT
	Reverse	CTCGTCACAAGCAGGGTTAAG
OPN	Forward	GGAGGAAACCAGCCAAGG
	Reverse	TGCCAGAATCAGTCACTTTCAC

2.5.1. Rat femoral defect model

All rats were anesthetized with injection of ketamine 100 mg/kg and xylazine 12.5 mg/kg. A 3 cm incision was made in the skin of the lateral thigh. The intermuscular space was separated carefully to avoid vascular injury. A unilateral cortical hole with 2 mm diameter was drilled in the femur to create bone bleeding. The hemostatic agent was immediately applied to the hole control bleeding management, while the control group was left untreated. The exuded blood was continuously wiped using a pre-weighted dry cotton ball (M_0). After 5 min, hemostasis was visually checked and the mass of the blood-absorbed cotton ball (M_1) was recorded. The amount of hemorrhage was calculated by M_1-M_0. Rats were sacrificed at the end of the experiment.

2.5.2. Rat calvarial defect model

All rats were anesthetized with injection of ketamine 100 mg/kg and xylazine 12.5 mg/kg. After shaving and disinfection, a 2 cm longitudinal incision was made in the middle of the skull, and soft tissue and periosteum were carefully separated. A hole with 5 mm diameter was drilled in the skull to create a bone defect model and the as-prepared putty was used to fill the bone cavity. The incision was sutured, and antibiotics were administered within 3 days after surgery.

At 4 and 8 weeks postoperatively, rats were sacrificed after anesthesia, and the calvarias were removed and fixed with 4 % paraformaldehyde. Specimens were scanned using a Micro-CT (SkyScan 1276, Bruker, Belgium) with voltage 50 kV, electricity 200 μA, and resolution 6 μm. The calvarial structures were reconstructed and a 5 mm diameter cylinder region of interest (ROI) containing 50 layers was selected to analyze percent bone volume (BV/TV), trabecular thickness (Tb.Th), and trabecular number (Tb.N) using software DataViewer, CTan, CTvol, and CTvox (Bruker, Belgium). The gray value was set as 80–255 and the despeckle command in the CTan software was used to sweep the residual undegraded material granules around the new forming bone.

Subsequently, after decalcification in EDTA at room temperature for 4 weeks, these specimens were dehydrated and embedded in paraffin. Histological sections were cut into 4 μm pieces using microtome (HistoCore MULTICUT, Leica). The steps of Hematoxylin and Eosin (H&E) staining included deparaffinization, Harris hematoxylin staining 10 min, acidic ethanol differentiation 5 s, reagent bluing 5 min, eosin staining 3 min, ethanol dehydration and xylene clearing. The steps of Masson staining included deparaffinization, hematoxylin staining 10 min, acidic ethanol differentiation 5 s, reagent bluing 5 min, ponceau fuchsin staining 10 min, phosphomolybdic acid solution washing 2 min, aniline blue staining 2 min, ethanol dehydration and xylene clearing. The steps of OPN immunohistochemical staining included deparaffinization, antigen retrieval with pepsin 37 °C 20 min, blocking endogenous peroxidase 10 min (dark), incubation with the primary antibody 4 °C overnight, reaction with amplification reagent 37 °C 20 min, incubation with enzyme-labeled polymer 37 °C 20 min, DAB staining, hematoxylin counterstaining 1 min, followed by dehydration and mounting. Sections were mounted with neutral balsam, and then captured using a digital slide scanner (Pannoramic Scan II, 3DHISTECH, Hungary).

2.6. Statistic analysis

Data are expressed as mean ± standard deviation (SD). The difference was statistically significant using t-test, and $p < 0.05$ was considered statistically significant.

3. Results

3.1. Characterizations of CaPBW

CaPBW prepared in current work showed great workability in hand, paving possibility in shape manipulation and irregular sized bone defect filling adaptation (Fig. 1A). The XPS spectra (Fig. 1C) show the peaks of

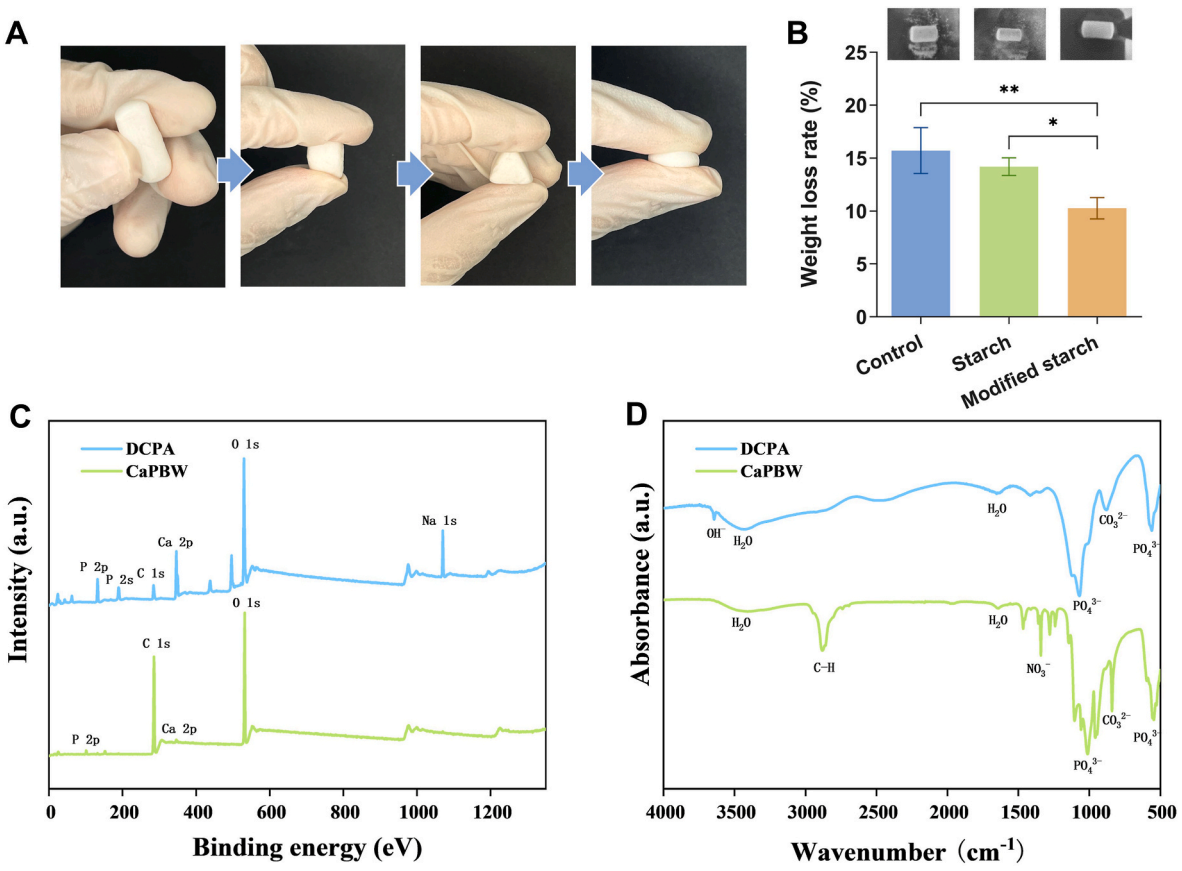

Fig. 1. CaPBW characterization and anti-collapsibility: (A) The as-prepared CaPBW can be shaped by hand; (B) Weight loss and structure integrity evaluation in shaking fluid of CaPBW (Modified Starch) and its counterparts in the absence of starch (Control) or using only pre-gelatinized starch (Starch); (C) XPS and (D) FTIR of DCPA and CaPBW. (*$p < 0.05$; **$p < 0.01$).

relevant elements in the DCPA and CaPBW samples. Compared to DCPA, the peaks for Ca and P in CaPBW are lower, while the C peak is higher. This can be attributed to the addition of starch and PEG, which encapsulate the DCPA and CPC, resulting in the reduced intensity of the other elemental peaks. The FTIR spectra of DCPA and CaPBW (Fig. 1D) display characteristic peaks for PO_4^{3-}, H_2O, and CO_3^{2-}. The presence of CO_3^{2-} may result from residual $NaHCO_3$ used in the reaction or CO_2 in air. Additionally, compared to DCPA, the CaPBW spectrum shows increased peaks for NO_3^- (originating from the starch crosslinker calcium nitrate) and C-H bonds from PEG.

Once in contact with physiological fluid, the PEG in the CaPBW matrix could be exchanged with water to further induce the hydrolysis reaction of CPC to gradually make CaPBW solid, along with the calcium ion modified cohesive high-amylopectin starch and DCPA granules forming a network to avoid disintegration of prepared CaPBW in dynamic aqueous environment. The mass loss rate of CaPBW was found to be about 10 %, attributed to the loss of PEG during PBS incubation. Meanwhile, in test group in the absence of starch or using only pre-gelatinized starch, specimen structure disintegration with weight loss above 15 % was witnessed after 10 min shaking (Fig. 1B). These observations implied the as-prepared CaPBW can be adaptable to irregular bone defect with fluid and generate a solid matrix in situ.

After self-curing in PBS for days, the compressive strength of hardened CaPBW revealed a gradual increase to 4.56 ± 0.43 MPa, comparable to reported value of cancellous bone (Fig. 2A and B). In addition, compressive mechanical curve of CaPBW showed the material exhibited plastic deformation at day 1 and then gradually changed to brittle fracture at day 5, indicating complete solidification of CaPBW in situ (Fig. 2C). This observation was in agreement of the phase processing of CPC, which takes days to finish calcium phosphate phase transition. The relevant degradation behavior study of CaPBW revealed a 40 % weight loss at day 10, accompanied with the pH value decreased from initial 7.1 ± 0.1 to 6.8 ± 0.1 (Fig. 2D). On one hand, the weight loss could be explained by the gradual dissolution of PEG and modified waxy starch in aqueous environment. In specific, the pre-gelatinization and presence of Ca^{2+} in matrix could enhance the rehydratability of the starch [22]. On the other hand, the mild pH change was suggested to be correlated with the DCPA in CaPBW, DCPA releases $HPO4^{2-}$ in situ, which supports its continuous degradation *in vivo* and provides a supersaturated supply of calcium and phosphate substrates [23]. However, this value was still in a safe neutral range relative to the human internal environment, unable to induce abnormal reactions such as inflammation. XRD was also performed to track the phase change of CaPBW in PBS, revealing gradual removal of PEG and formation of hydroxyapatite, which was in agreement with the CaPBW solidification mechanism (Fig. 2E). The micro-morphology change of CaPBW with time was shown in Fig. 2F, in which a transition from irregular sized particles to plate-like crystals was seen during 1–5 days. This phenomenon could be explained by the precipitation of hydroxyapatite during the hydrolysis of CPC precursors [24], which consequently forming an organized crystal network to provide mechanical support of CaPBW. The chemical reaction is as follows:

Dissolution: $3Ca_3(PO_4)_2 + 6H_2O \rightarrow 9Ca^{2+} + 6HPO_4^{2-} + 6OH^-$

Precipitation: $9Ca^{2+} + 6HPO_4^{2-} + 6OH^- \rightarrow Ca_9(HPO_4)\ (PO_4)_5(OH) + 5H_2O$

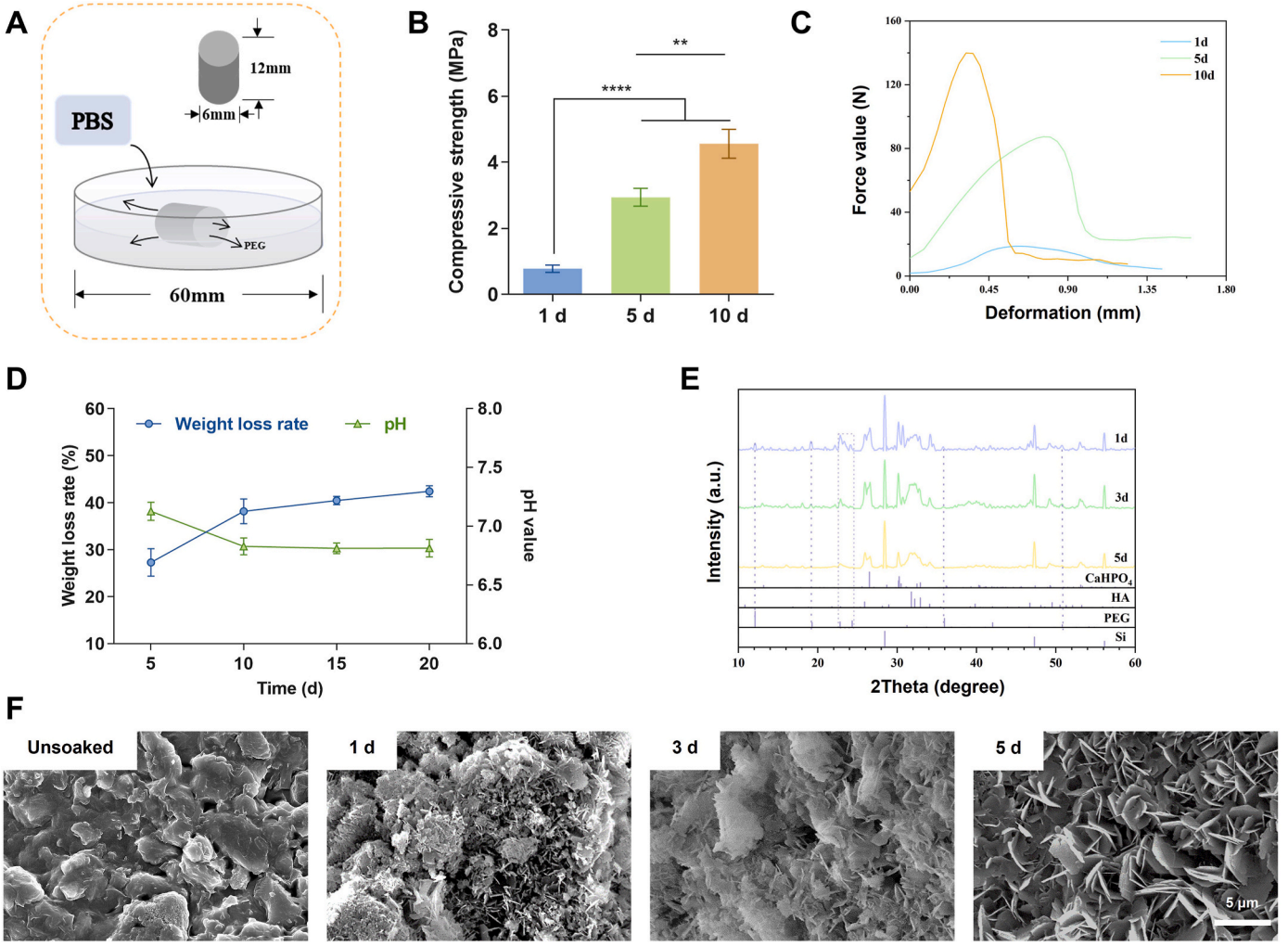

Fig. 2. Physicochemical properties change of CaPBW with time during self-curing: (A) schematic of PEG and water exchange induced solidification of CaPBW in fluid; (B) compressive strength; (C) compressive mechanical curve; (D) weight loss and pH change in PBS; (E) XRD patterns; (F) micromorphology characterized using SEM. (**p < 0.01; ****p < 0.0001).

3.2. Hemostasis ability evaluation

The liquid sealing evaluation using a water-filled acrylic tube showed that both CaPBW and bone wax effectively prevented water leakage at a pressure of 140 mmHg for 7 days. Similarly, in tests with fresh pig long bones, both materials adhered to wet bone defects and blocked water flow for over 30 min. Water contact angle results of CaPBW (23.9 ± 4.8°) and bone wax (110.1 ± 8.5°) were shown in Fig. 3A, indicting CaPBW can provide a hydrophilic surface for blood cells adherence and coagulation activation. SEM (Fig. 3B) showed that on the surface of CaPBW large amounts of platelets and fibrin networks were observed, as an alternative to the rarely found platelets on bone wax. The clotting time (Fig. 3C) showed no significant changes in APTT and PT for both bone wax and CaPBW compared to the blank control group, indicating that neither sample had a notable effect on the intrinsic or extrinsic coagulation pathways. However, TEG (Fig. 3D) revealed a significant reduction in reaction time (R value) after treatment with both CaPBW and bone wax, suggesting that both samples strongly activated the coagulation cascade, inducing a hypercoagulable state and rapidly initiating clot formation. Additionally, the R value for CaPBW was lower than that of bone wax, indicating that CaPBW was more effective in activating the coagulation cascade. The α angle for both CaPBW and bone wax was significantly larger than that of the control group, indicating that both samples accelerated the rate of blood clot formation. On the other hand, the maximum amplitude (MA), which reflects clot strength, was slightly lower for CaPBW compared to bone wax. This may be related to CaPBW's water absorption properties and the slight disintegration of the sample into powder.

In addition, hemolysis results of bone wax (0.017 %) and CaPBW (0.008 %) are shown in Fig. 3E, both showing significant difference to water group. In medical practice, degree of hemolysis is acknowledged as a sensitive indicator for assessing red blood cell damage, and hemolysis index lower than 2 % is defined as no hemolysis. Therefore, CaPBW could be considered as hemocompatible agent for bleeding control.

3.3. In vitro cellular tests

The proliferation of MC3T3-E1 cells cultured in CaPBW and bone wax extracts at 1 and 3 days showed no significant difference in cell viability, confirming the cytocompatibility of the materials (Fig. 4A). Similarly, few dead cells labeled by red fluorescence were seen in the live/dead staining results (Fig. 4B).

To verify the osteogenic differentiation ability of CaPBW, MC3T3-E1 cells were cultured using osteogenic-inducing extracts and were tested for ALP staining and ARS staining. The CaPBW group showed the highest number of positive ALP staining cells at 7 days compared to the control and bone wax groups (Fig. 5A). Moreover, the CaPBW group showed the highest red calcium depositions among all test groups in the ARS

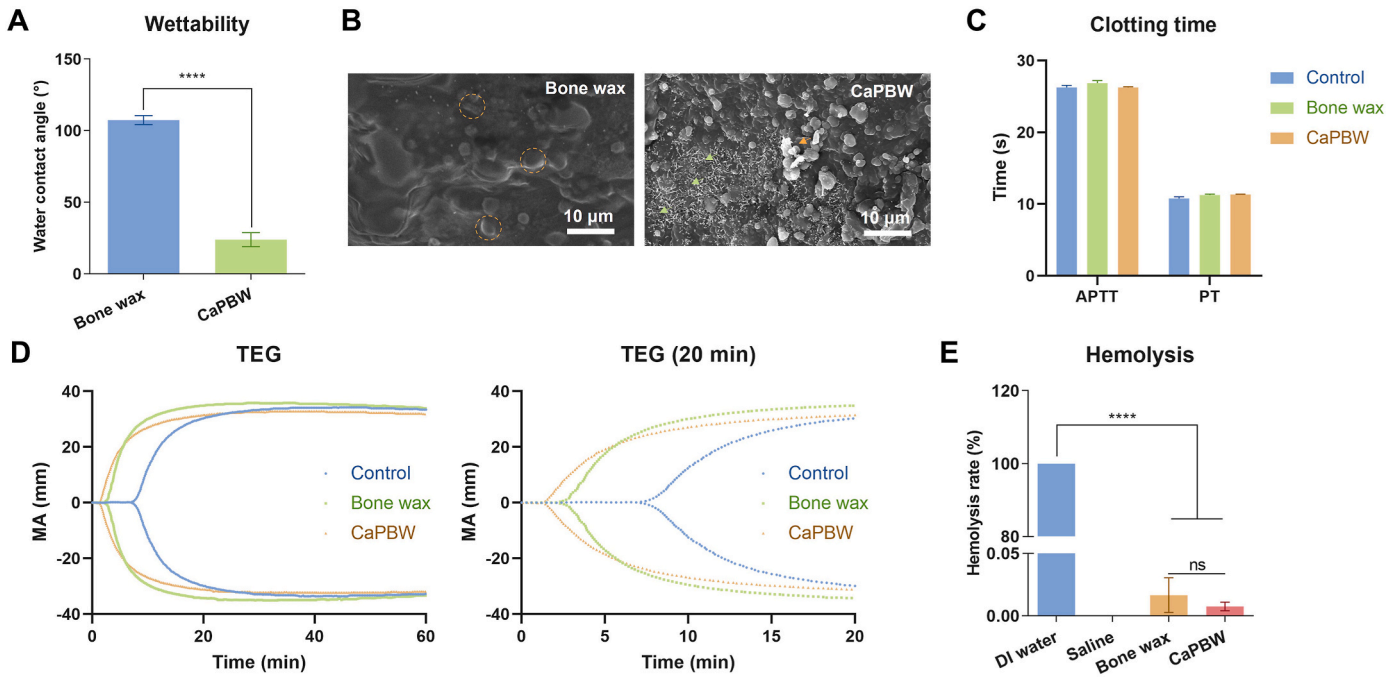

Fig. 3. Hemostasis ability evaluation of CaPBW: (A) water contact angle; (B) SEM characterization of bone wax and CaPBW surface after exposure to blood; (C) APTT and PT clotting time; (D) Thromboelastography (TEG) and the first 20 min of TEG; (E) Hemolysis test result of specimens. (ns, no significant difference; **p < 0.01; ****p < 0.0001).

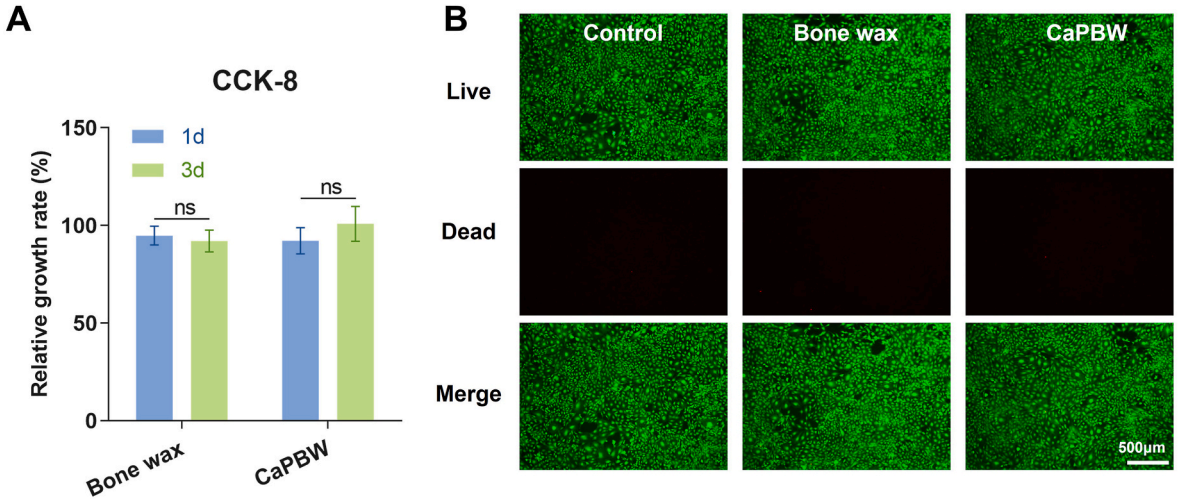

Fig. 4. Cell proliferation study: (A) the relative growth rate of CCK-8 assay, n = 9 per group per timepoint; (B) typical image of live/dead staining after 3 days cell proliferation. (ns, no significant difference).

staining at 14 days (Fig. 5B). The semiquantitative analysis of ARS staining by adding cetylpyridine solution showed that the stained calcium depositions were almost doubled in the CaPBW group as compared to its counterparts, which was consistent with the staining results (Fig. 5C). Further, RT-qPCR was performed to investigate the effect of CaPBW on the expression of osteogenesis-related genes in MC3T3-E1 cells. After 7 days of osteogenesis induction, the expression of OCN and OPN increased by 2.84 and 3.67 folds in the CaPBW group compared with the control group respectively, while there was no significant difference in the bone wax group and the control one (Fig. 5D). These results indicated CaPBW was able to upregulate osteogenic differentiation in osteoblasts, capable of providing a favored microenvironment for bone regeneration.

3.4. *In vivo* evaluations of hemostasis and osteogenesis

The *in vivo* hemostasis potential of CaPBW was assessed using a rat femoral defect model (Fig. 6A), in which the amount of blood absorbed on cotton balls within 5 min was used as an indicator reflecting bleeding control capability. As shown in Fig. 6B, blood loss was greatly reduced in CaPBW group (0.074 ± 0.120 g) and bone wax group (0.145 ± 0.162 g) as compared to the control group (1.063 ± 0.083 g). Therefore, CaPBW was confirmed to be a reliable alternative to bone wax, capable of sealing bleeding bone defect and achieving hemostasis in situ.

In spite of the hemostasis evaluation, the bone regenerative potential of CaPBW was also tested using a rat calvarial defect model. Micro-CT scanning and quantitative analysis were performed on calvarial specimens at 4 and 8 weeks to evaluate new bone formation level. We

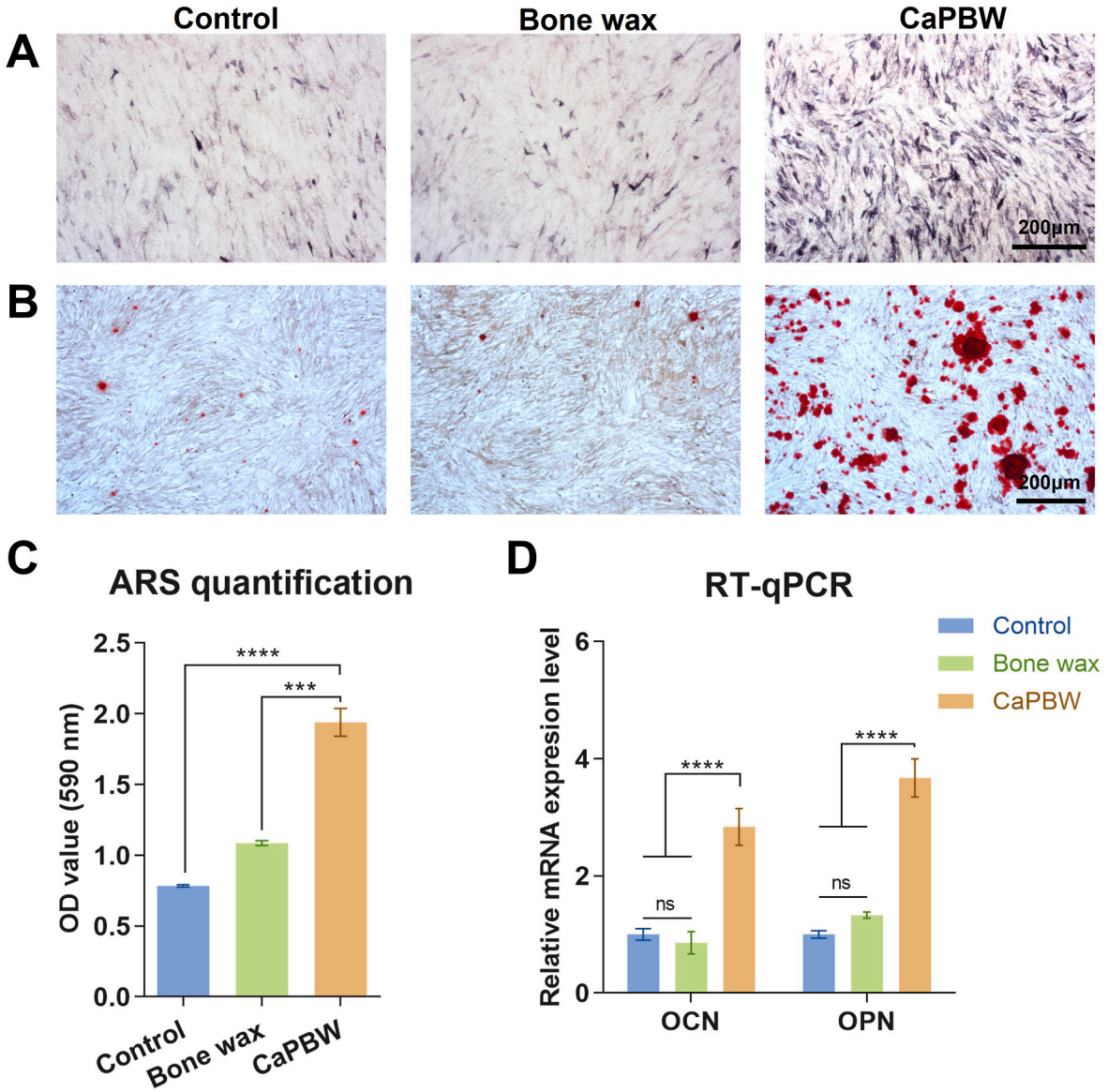

Fig. 5. *In vitro* osteogenic differentiation ability evaluation: (A) ALP staining at 7 day; (B) ARS staining at 14 day; (C) quantification of mineral deposition by detecting absorbance of ARS extracts, n = 3 per group; (D) RT-qPCR analysis of the relative mRNA expression. (ns, no significant difference; ***p < 0.001; ****p < 0.0001).

reconstructed the ROI area in 3D and color-coded the regions of new bone formation, in which CaPBW group exhibited significantly enhanced new bone formation compared to the blank group. In contrast, the non-degradable bone wax group showed poorer new bone formation than the blank group, as bone wax occupied the osteogenic space. Furthermore, regarding the density similarity of residual CaPBW and bone, a despeckle command in the CTan software was used to sweep speckles that were not bonded to the bone tissue (the red part in Fig. 6C) and calculate parameters of the residual new bone (the yellow part in Fig. 6C). However, due to the software limitation, some dissociative new bone might be swept and resulted in smaller measured values than the actual values in CaPBW group. Nevertheless, CaPBW group still revealed the highest new bone formation among all test groups. The quantitative results showed that the CaPBW group had significantly higher BV/TV, Tb.Th, and Tb.N than the other two groups (Fig. 6D–F). On contrast, bone wax interferes with normal bone repair due to its inert nature. All these results indicates that CaPBW can provide a temporary platform for osteogenesis.

H&E and Masson staining were performed on calvarial specimens at 4 and 8 weeks, respectively (Fig. 7A and B). The defects in the control group were mainly composed of fibrous tissue junctions at 4 weeks, and no obvious bone healing was observed at 8 weeks. In the CaPBW group, a large area of new bone could be observed in the defect area at 4 weeks, with new bone formation and maturation shown by blue and red in Masson staining. At 8 weeks, new bone bridging in the defect could be observed. Moreover, formation of crescent-shaped new bone around the residual particles was observed in Masson staining. On the other hand, fibrous tissue growth was seen around the nondegradable bone wax, forming collar-like structures at 4 weeks. Subsequently, a mass of abnormal fibrous tissue was witnessed around bone wax at 8 weeks post-surgery, indicating occurrence of inflammation caused by bone wax in situ. These histological results thereby confirmed the superiority of CaPBW to bone wax in bone regeneration. At 8 weeks, immunohistochemical staining (Fig. 7C) revealed significant OPN staining in the bone formation areas of the CaPBW group, while no noticeable positive staining was observed in the other two groups.

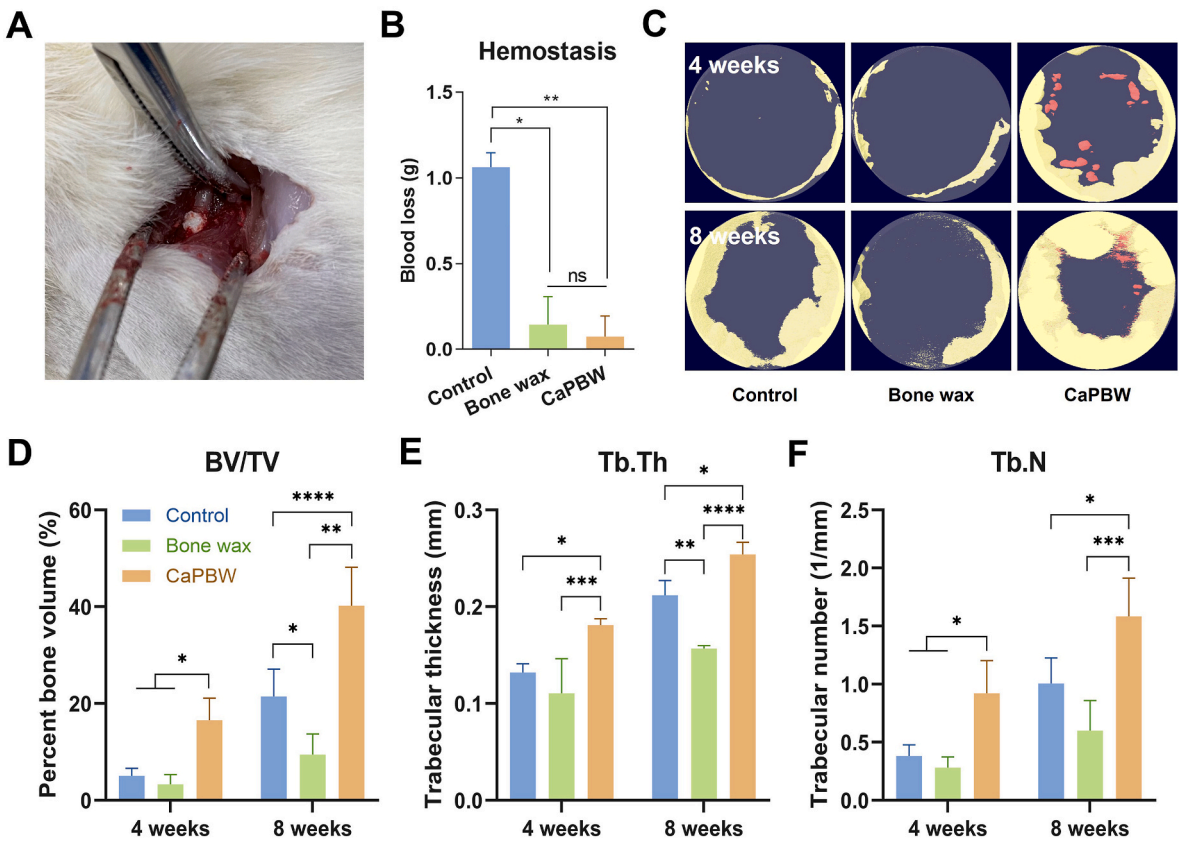

Fig. 6. *In vivo* hemostasis and osteogenesis capability evaluation: (A) CaPBW induced immediate bleeding control in rat femoral defect. (B) Evaluation of the hemostatic effect of different materials by blood loss, n = 3 per group. (C) Micro-CT 3D reconstructed new bone (yellow) and some residual material (red) in the ROI (5 mm diameter). Quantitative analysis of BV/TV (D), Tb.Th (E), and Tb.N (F), n = 3 per group per timepoint.

4. Discussion

Exploration of reliable hemostatic agent with bone wax-like handling characteristic for bleeding bone management lasts for decades [17]. Unfortunately, candidates such as malleable organic putty or bioceramic cement-based paste failed to adapt to either osteogenesis requirement or surgical procedure in medical practice. In the present study, a self-curing cement and premixed design integrated material, CaPBW, was developed for bone wax substitution. The corresponding investigations proved CaPBW could provide an attractive ready-to-use platform for hemostasis, temporary physical support, bone repairing, along with preservation of bone wax-like manipulation advantages.

As demonstrated in materials section, the CaPBW was formulated of CPC, DCPA granules, modified starch and PEG, all playing vital roles in performance regulation. CPC is a traditional bone repairing cement, highlighted with advantages in self-hardening and osteogenesis stimulation. However, CPC alone was reported to exhibit limited anti-collapse ability in aqueous environment and setting time restriction during operation. Therefore, modified starch and PEG were introduced for its structure integrity improvement and operation time restriction removal, making it more adaptable to bone bleeding control practice. On one hand, the modified starch used in current work was a ionically cross-linked viscous hydrogel with calcium and nitrate ions present in starch hydrogel network, reported to exhibit soft/hard tissue adhesiveness, high stretch-ability, self-healing capability, cytocompatibility, low hemolysis risk, strong antibacterial effect, and degradability [25]. These properties thereby endow CPC anti-collapse and hemostasis reinforcement, making it more reliable in bleeding site. On the other hand, PEG paved the possibility to initiate CPC solidification when used to seal bleeding wound, paving possibility of immediate control of sudden bleeding during surgery in the absence of setting time restriction.

To further improve the performance of CaPBW in situ, DCPA granules were used as another component. As compared to hydroxyapatite, the end phase of CPC after hydration, DCPA was known to favor osteointegration and osteoconduction, along with revealing a better balance between implant resorption and new bone formation as compared to its counterparts [23]. CPC was known to lack macropores favored for bone in-growth, consequently comprising its regeneration ability [26]. Therefore, strategies such as adding soluble porogen agents [27] or gas foaming [28] were developed, purposed to generate high porosity and macropores in CPC. However, there is a controversy between early mechanical stability and high porosity generated in these methods. On contrast, regarding its bone formation adaptable resorption, DCPA granules could serve as a mechanical support post-surgery and a sacrificing agent for porosity generation during bone in-growth.

The hemostatic mechanism of CaPBW material likely involves mechanical tamponade, the water absorption properties of starch and PEG, and the activation of coagulation by the release of Ca ions. Experimental results showed no significant changes in APTT and PT for both CaPBW and bone wax, indicating no noticeable effect on the intrinsic or extrinsic coagulation pathways, confirming that the release of Ca ions (clotting factor IV) has a negligible role in coagulation activation. However, TEG results demonstrated that CaPBW initiated coagulation faster than bone wax, likely due to its hydrophilic surface and water absorption properties. Of course, the primary mechanism is likely mechanical tamponade, which is regarded as the fastest and most effective method of intraoperative hemostasis by clinicians. The resulting hemodynamic change is also a critical factor for coagulation to occur.

Different from bone wax, the components in CaPBW such as starch and calcium phosphates are reported to show high affinity to blood and its proteins [29,30]. With progressed understanding of bone regeneration process, it is acknowledged the blood clotting induced hematoma

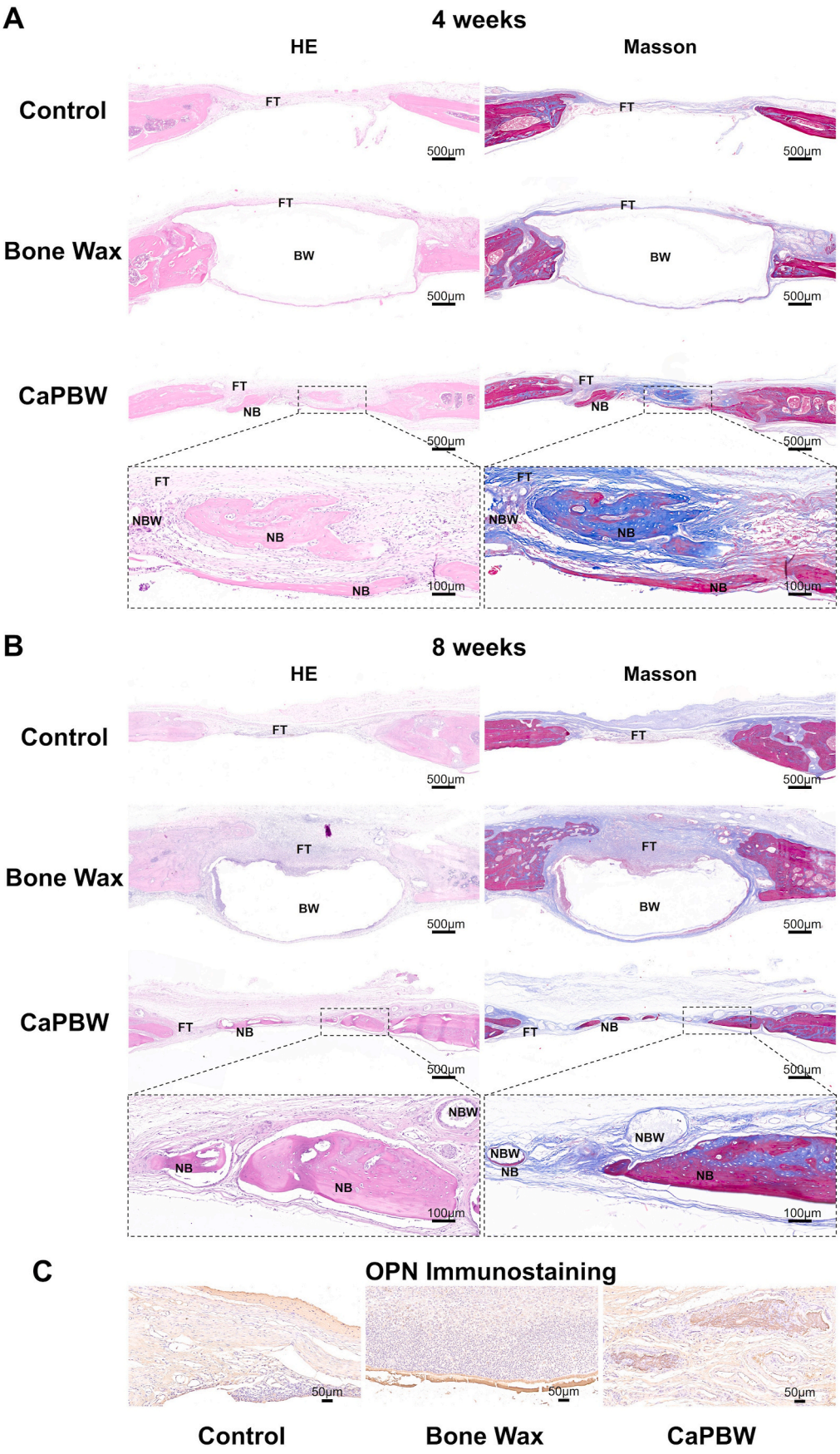

Fig. 7. Histology staining of calvarial defect repair: HE and Masson staining were performed on each group at 4 (A) and 8 (B) weeks, respectively. New bone area in the CaPBW group was enlarged for detail observation. (C) Immunohistochemistry (IHC) staining of OPN at 8 weeks. FT: fibrous tissue, BW: bone wax, CaPBW: residual implanted material, NB: new bone.

play vital role in bone regeneration. As reported in literature, fracture hematoma could induce ectopic bone formation, along with up-regulation of IL6, IL8, VEGF, CXCR4, SPP1 and RUNX2 expressions for bone healing promotion [31]. Besides, coagulated blood and fibrinolysis formation on material surface could regulate activity of macrophages as well as boost bone regeneration through promoting the formation of blood vessels [32]. In addition, Yin and his colleagues found co-culture with macrophages on the blood clot or in the clot-conditioned medium could down-regulate the inflammation and manipulate a favorable osteoimmunomodulatory environment for osteogenesis [33]. Therefore, it is speculated in spite of the intrinsic osteogenesis capability of CaPBW, its absorbed blood and as-formed hematoma also made great contribution to bone healing after hemostasis. Inspired by these events, CaPBW formula can be further tailored to provide a more effective platform accelerating bone regeneration via regulating micro-environment during defect healing process. For instance, using DCPA particles and CPC as localized delivery system to load osteogenic or angiogenic drugs could enhance the osteoinduction capability of the material, offering better potential as a drug/device combination medical implant for large area bone defect repair [34]. Alternatively, incorporating therapeutic drugs such as metformin into the material could enable in situ drug release, targeting the treatment of specific defects like diabetic bone deficiencies [35]. This could be the next step in the development of CaPBW materials.

5. Conclusion

In this study, ready-to-use CaPBW was formulated by the incorporation of CPC, DPCA granules, modified starch and PEG for bleeding bone management. As compared to traditional bone hemostatic agent bone wax, CaPBW not only preserved its advantages in handling and defect sealing, but also provided platform for temporary physical support and bone regeneration acceleration, as confirmed in both *in vitro* and *in vivo* investigations. Firstly, CaPBW putty showed feasibility in shape manipulation to adapt to irregular bone defect, along with high physiological fluid resistance for wound closure. Subsequently, the exchange between PEG and water could induce self-hardening of CaPBW via the solidification of CPC with starch and DCPA granules, providing a temporary scaffold in situ for bleeding control. As the time progressed, CaPBW could be gradually absorbed and simultaneously enhance bone regeneration, revealing impressive *in vivo* outcomes as compared to blank control and bone wax. Thus, CaPBW is a promising hemostatic and bone regenerative agent for bleeding bone management.

Funding/support statement

National Natural Science Foundation of China (82025025, U23A6008), National Key Research and Development Program of China (2023YFC2412300), Natural Science Foundation of Hebei Province of China (C2021202003, H2022202007), Natural Science Foundation of Tianjin of China (21JCZDJC01110), Full-time Talents Program of Hebei Province of China (2020HBQZYC012), Academician Expert Workstation of Yunnan Province of China (202205AF150025), The Scientific Research Project of Tianjin Education Commission (2022KJ096), The Tianjin Health Research Project (TJWJ2023QN051)

Conflicts of interest

A conflict of interest occurs when an individual's objectivity is potentially compromised by a desire for financial gain, prominence, professional advancement or a successful outcome. The Editors of the *Journal of Orthopaedic Translation* strive to ensure that what is published in the Journal is as balanced, objective and evidence-based as possible. Since it can be difficult to distinguish between an actual conflict of interest and a perceived conflict of interest, the Journal requires authors to disclose all and any potential conflicts of interest.

Acknowledgements

All persons who have made substantial contributions to the work reported in the manuscript (e.g., technical help, writing and editing assistance, general support), but who do not meet the criteria for authorship, are named in the Acknowledgements and have given us their written permission to be named. If we have not included an Acknowledgements, then that indicates that we have not received substantial contributions from non-authors.

References

[1] Wang W, Yeung KWK. Bone grafts and biomaterials substitutes for bone defect repair: a review. Bioact Mater 2017;2:224–47. https://doi.org/10.1016/j.bioactmat.2017.05.007.
[2] Fernandez de Grado G, Keller L, Idoux-Gillet Y, Wagner Q, Musset A-M, Benkirane-Jessel N, et al. Bone substitutes: a review of their characteristics, clinical use, and perspectives for large bone defects management. J Tissue Eng 2018;9:2041731418776819. https://doi.org/10.1177/2041731418776819.
[3] Calori GM, Mazza E, Colombo M, Ripamonti C. The use of bone-graft substitutes in large bone defects: any specific needs? Injury 2011;42(Suppl 2):S56–63. https://doi.org/10.1016/j.injury.2011.06.011.
[4] Jin C, Song E-K, Santoso A, Ingale PS, Choi I-S, Seon J-K. Survival and risk factor analysis of medial open wedge high tibial osteotomy for unicompartment knee osteoarthritis. Arthroscopy 2020;36:535–43. https://doi.org/10.1016/j.arthro.2019.08.040.
[5] Belsey J, Yasen SK, Jobson S, Faulkner J, Wilson AJ. Return to physical activity after high tibial osteotomy or unicompartmental knee arthroplasty: a systematic review and pooling data analysis. Am J Sports Med 2021;49:1372–80. https://doi.org/10.1177/0363546520948861.
[6] Palanisamy JV, Das S, Moon KH, Kim DH, Kim TK. Intravenous tranexamic acid reduces postoperative blood loss after high tibial osteotomy. Clin Orthop Relat Res 2018;476:2148–54. https://doi.org/10.1097/CORR.0000000000000378.
[7] Kim K-I, Kim HJ, Kim GB, Bae SH. Tranexamic acid is effective for blood management in open-wedge high tibial osteotomy. Orthop Traumatol Surg Res 2018;104:1003–7. https://doi.org/10.1016/j.otsr.2018.07.019.
[8] Martin R, Birmingham TB, Willits K, Litchfield R, Lebel M-E, Giffin JR. Adverse event rates and classifications in medial opening wedge high tibial osteotomy. Am J Sports Med 2014;42:1118–26. https://doi.org/10.1177/0363546514525929.
[9] Ogawa H, Matsumoto K, Akiyama H. The prevention of a lateral hinge fracture as a complication of a medial opening wedge high tibial osteotomy: a case control study. Bone Joint Lett J 2017;99-B:887–93. https://doi.org/10.1302/0301-620X.99B7.BJJ-2016-0927.R1.
[10] Imhoff FB, Imhoff AB. Editorial commentary: lateral hinge fracture in high tibial osteotomy: risk or annex? Arthroscopy 2018;34:3080–1. https://doi.org/10.1016/j.arthro.2018.08.016.
[11] van den Bekerom MPJ, Patt TW, Kleinhout MY, van der Vis HM, Albers GHR. Early complications after high tibial osteotomy: a comparison of two techniques. J Knee Surg 2008;21:68–74. https://doi.org/10.1055/s-0030-1247797.
[12] Lash NJ, Feller JA, Batty LM, Wasiak J, Richmond AK. Bone grafts and bone substitutes for opening-wedge osteotomies of the knee: a systematic review. Arthroscopy 2015;31:720–30. https://doi.org/10.1016/j.arthro.2014.09.011.
[13] Jung W-H, Takeuchi R, Kim D-H, Nag R. Faster union rate and better clinical outcomes using autologous bone graft after medial opening wedge high tibial osteotomy. Knee Surg Sports Traumatol Arthrosc 2020;28:1380–7. https://doi.org/10.1007/s00167-019-05463-w.
[14] Van Genechten W, Van den Bempt M, Van Tilborg W, Bartholomeeusen S, Van Den Bogaert G, Claes T, et al. Structural allograft impaction enables fast rehabilitation in opening-wedge high tibial osteotomy: a consecutive case series with one year follow-up. Knee Surg Sports Traumatol Arthrosc 2020;28:3747–57. https://doi.org/10.1007/s00167-019-05765-z.
[15] Putnis S, Neri T, Klasan A, Coolican M. The outcome of biphasic calcium phosphate bone substitute in a medial opening wedge high tibial osteotomy. J Mater Sci Mater Med 2020;31:53. https://doi.org/10.1007/s10856-020-06391-9.
[16] Choi WC, Kim B, Kim U, Lee Y, Kim J-H. Gap healing after medial open-wedge high tibial osteotomy using injectable beta-tricalcium phosphate. J Orthop Surg 2017;25:2309499017727942. https://doi.org/10.1177/2309499017727942.
[17] Zhou H, Ge J, Bai Y, Liang C, Yang L. Translation of bone wax and its substitutes: history, clinical status and future directions. J Orthop Translat 2019;17:64–72. https://doi.org/10.1016/j.jot.2019.03.005.
[18] Liu C, Liu Z, Wang K, Sun Y, Liu Q, Sun X, et al. Novel bone wax based on DCPA granules and modified starch for hemostasis and bone regeneration. Appl Mater Today 2023;32:101815. https://doi.org/10.1016/j.apmt.2023.101815.
[19] Liu H, Zhang Z, Gao C, Bai Y, Liu B, Wang W, et al. Enhancing effects of radiopaque agent BaSO4 on mechanical and biocompatibility properties of injectable calcium phosphate composite cement. Mater Sci Eng C 2020;116:110904. https://doi.org/10.1016/j.msec.2020.110904.
[20] Vajgel A, Mardas N, Farias BC, Petrie A, Cimões R, Donos N. A systematic review on the critical size defect model. Clin Oral Implants Res 2014;25:879–93. https://doi.org/10.1111/clr.12194.

[21] McGovern JA, Griffin M, Hutmacher DW. Animal models for bone tissue engineering and modelling disease. Dis Model Mech 2018;11:dmm033084. https://doi.org/10.1242/dmm.033084.
[22] Xi W, Liu P, Ling J, Xian D, Wu L, Yuan Y, et al. Pre-gelatinized high-amylose starch enables easy preparation of flexible and antimicrobial composite films for fresh fruit preservation. Int J Biol Macromol 2024;254:127938. https://doi.org/10.1016/j.ijbiomac.2023.127938.
[23] Zhou H, Yang L, Gbureck U, Bhaduri SB, Sikder P. Monetite, an important calcium phosphate compound-Its synthesis, properties and applications in orthopedics. Acta Biomater 2021;127:41–55. https://doi.org/10.1016/j.actbio.2021.03.050.
[24] Ginebra M-P, Canal C, Espanol M, Pastorino D, Montufar EB. Calcium phosphate cements as drug delivery materials. Adv Drug Deliv Rev 2012;64:1090–110. https://doi.org/10.1016/j.addr.2012.01.008.
[25] Mao Y, Li P, Yin J, Bai Y, Zhou H, Lin X, et al. Starch-based adhesive hydrogel with gel-point viscoelastic behavior and its application in wound sealing and hemostasis. J Mater Sci Technol 2021;63:228–35. https://doi.org/10.1016/j.jmst.2020.02.071.
[26] Qian G, Lu T, Zhang J, Liu R, Wang Z, Yu B, et al. Promoting bone regeneration of calcium phosphate cement by addition of PLGA microspheres and zinc silicate via synergistic effect of in-situ pore generation, bioactive ion stimulation and macrophage immunomodulation. Appl Mater Today 2020;19:100615. https://doi.org/10.1016/j.apmt.2020.100615.
[27] Takagi S, Chow LC. Formation of macropores in calcium phosphate cement implants. J Mater Sci Mater Med 2001;12:135–9. https://doi.org/10.1023/a:1008917910468.
[28] del Real RP, Wolke JGC, Vallet-Regí M, Jansen JA. A new method to produce macropores in calcium phosphate cements. Biomaterials 2002;23:3673–80. https://doi.org/10.1016/s0142-9612(02)00101-1.
[29] Zheng C, Bai Q, Wu W, Han K, Zeng Q, Dong K, et al. Study on hemostatic effect and mechanism of starch-based nano-microporous particles. Int J Biol Macromol 2021;179:507–18. https://doi.org/10.1016/j.ijbiomac.2021.03.037.
[30] Kikuchi L, Park JY, Victor C, Davies JE. Platelet interactions with calcium-phosphate-coated surfaces. Biomaterials 2005;26:5285–95. https://doi.org/10.1016/j.biomaterials.2005.01.009.
[31] Kolar P, Gaber T, Perka C, Duda GN, Buttgereit F. Human early fracture hematoma is characterized by inflammation and hypoxia. Clin Orthop Relat Res 2011;469:3118–26. https://doi.org/10.1007/s11999-011-1865-3.
[32] Lu H, Xiao L, Wang W, Li X, Ma Y, Zhang Y, et al. Fibrinolysis regulation: a promising approach to promote osteogenesis. Tissue Eng Part B 2022;28:1192–208. https://doi.org/10.1089/ten.TEB.2021.0222.
[33] Bai L, Zhao Y, Chen P, Zhang X, Huang X, Du Z, et al. Targeting early healing phase with titania nanotube arrays on tunable diameters to accelerate bone regeneration and osseointegration. Small 2021;17:e2006287. https://doi.org/10.1002/smll.202006287.
[34] Cao H, Li L, Li L, Meng X, Liu Y, Cheng W, et al. New use for old drug: local delivery of puerarin facilitates critical-size defect repair in rats by promoting angiogenesis and osteogenesis. J Orthop Translat 2022;36:52–63. https://doi.org/10.1016/j.jot.2022.05.003.
[35] Li H, Mao B, Zhong J, Li X, Sang H. Localized delivery of metformin via 3D printed GelMA-Nanoclay hydrogel scaffold for enhanced treatment of diabetic bone defects. J Orthop Translat 2024;47:249–60. https://doi.org/10.1016/j.jot.2024.06.013.